Research Article

Journal of Environmental Nanotechnology

Ultrasound-assisted Synthesis of YbSnO Nanoparticles Embedded in Nanofiber Composites for Biomedical Applications

M. Moniga[1], Mani Sivakumar[1] and Palati Sinduja[2*]

[1]Department of Pathology, Saveetha Dental College and Hospital, Saveetha Institute of Medical and Technical Sciences, Saveetha University, Chennai, TN, India

[2]Department of Oral and Maxillofacial Pathology, Saveetha Dental College and Hospital, Saveetha Institute of Medical and Technical Sciences, Saveetha University, Chennai, TN, India

Received: 08.05.2025 Accepted: 18.06.2025 Published: 30.06.2025

*sindujap.sdc@saveetha.com

ABSTRACT

Cancer remains one of the leading causes of mortality globally, with oral squamous cell carcinomas being significantly impacted by various risk factors, including tobacco and alcohol use, infections, and nutritional deficiencies. Despite advancements, ccurrent diagnostic and therapeutic approaches often have limitations, necessitating the need for novel approaches that enhance treatment efficacy while minimizing adverse effects. In this context, Ytterbium Tin Oxide (YbSnO) nanoparticles were synthesized via a wet chemical method and subsequently integrated into nanofiber cellulose (NFC) composites. The resulting YbSnO/NFC composites were characterized using X-ray diffraction, Fourier-transform infrared spectroscopy and field emission scanning electron microscopy (FE-SEM). The FE-SEM images revealed uniform dispersion of YbSnO nanoparticles within the NFC matrix. Cytotoxicity assays indicated a dose-dependent reduction in cell viability, with YbSnO@NFC composites exhibiting the highest cytotoxicity ($p < 0.05$), suggesting enhanced interactions between the components. Then the Gene expression by RT-PCR was examined in A549 cells seeded at a density of 5×10^6 cells per well in 100 mm culture plates. After overnight incubation, total RNA was extracted using the Total RNA Isolation Reagent (TRIR; Abgene, UK). These findings support the promising potential of YbSnO/NFC composites in biomedical applications, particularly in targeted cancer therapies.

Keywords: YbSnO nanoparticles; Ultrasound-assisted synthesis; Nanofiber composites; Antimicrobial activity; Biological applications.

1. INTRODUCTION

Recently, it has been recognized that cancer involves abnormal cell growth that can lead to the development of tumors that may spread to other parts of the body (Beheshti *et al.* 2021). The invasion-driven spread of tumors results in the formation of discontinuous secondary tumor masses, known as metastasis, which occur at sites where the cancer cells have lodged. The cancer death rate is rising rapidly in both developing and developed countries (Siegel *et al.* 2024). Cancer is the leading cause of mortality in the United States for individuals under 85 years old (Almalki *et al.* 2023). Numerous risk factors may lead to the development of oral squamous cell carcinomas (Dsouza *et al.* 2018). Some of the common factors that can lead to cancer include, use of tobacco, high alcohol intake, smoking, smokeless tobacco like snuff, use of mouthwash with higher alcohol content, high energy radiation, high exposure to sunlight, infections like Hepatitis B, Hepatitis C, Helicobactor pylori, HPV virus, Epstein-Barr virus, poor oral hygiene and poor nutrition. Inherited risk factors can account for up to 4% of all cancers (Huang *et al.* 2024). Reducing the excessive alcohol consumption and tobacco use may reduce the risk of oral cancer worldwide (Umapathy *et al.* 2023). Regular oral cancer screening by the dentist may facilitate early detection. However, people living in slum areas or rural areas may not be aware of cancer and often have limited access to dental treatment (Preet *et al*. 2024).

Dentists may face challenges in distinguishing between benign and malignant lesions through clinical examination alone. In such cases, advanced diagnostic techniques such as computerized tomography (CT) scans, bone scans, magnetic resonance imaging (MRI), positron emission tomography (PET), ultrasound and X-rays and biopsies are employed. Among these, biopsy is considered a standard procedure for definitive diagnosis, involving the collection of tissue samples for laboratory analysis. However, biopsies can sometimes be limited by insufficient tissue quantity or sampling errors, and repeated procedures may not always be feasible (Mira *et al.* 2024). Computerized tomography scan, although valuable, expose patients to ionizing radiation, potentially increasing the long-term risk of cancer (Saran

et al. 2024). Similarly, radiotherapy, while targeting localized cancer regions, can cause various side effects such as hair loss, skin irritation, dry mouth, sore throat and gastrointestinal discomfort, and bladder issues, depending on the site of exposure.

On the other hand, chemotherapy not only kills fast-growing cancer cells but also kills or slows the growth of healthy cells, leading to adverse effects such as hair loss, anaemia, severe nausea, mucosal ulcers, and cognitive difficulties (Lewis *et al.* 2025). Given these limitations, the development of alternative treatment modalities is essential. In this context, we propose the use of binary metal oxide nanoparticles combined with biopolymers, particularly focusing on their anticancer properties.

Metal and metal oxide nanoparticles play an important role in biomedicine due to their unique physicochemical properties (Shabatina *et al.* 2022). Ranging in size from 1 to 100 nm, nanoparticles are composed of natural or synthetic polymers (Shabatina *et al.* 2023). They can easily penetrate biological tissues (Neto *et al.* 2018). They are widely used across disciplines such as materials science, biotechnology, and environmental science (Bhatti *et al.* 2022) and have applications in both prophylactic and therapeutic vaccines (Zhao *et al.* 2014).

There are two types of nanoparticles: polymeric nanoparticles and inorganic nanoparticles. synthetic polymers are used to form nanoparticles such as poly(l-lactic acid) (PLA) and poly(lactic-co-glycolic acid) (PLGA) nanoparticles and poly(d, l-lactide-co glycolide) [PLG] nanoparticles (Kim *et al.* 1999; Thomas *et al.* 2011 and Silva, *et al.* 2013). Natural polymers, including pullulan, alginate, and chitosan, offer advantages such as biocompatibility, biodegradability, and low toxicity (Borges *et al.* 2008; Li *et al.* 2013; Zhao *et al.* 2014). For enhanced thermal properties and structural integrity, nano-additives are incorporated into polymer matrices using in situ polymerization, melt blending, or solution casting techniques (Tsakiridou *et al.* 2024).

Ytterbium tin oxide nanoparticles exhibit remarkable optical, electrical, and chemical properties (Rajakumar *et al.* 2021; Cheng, *et al.* 2016; Dheyab *et al.* 2021). When integrated with nanofiber composites, YbSnO nanoparticles improve both structural and biological functionalities (Vasudevan *et al.* 2023; Montalvão *et al.* 2024; Kaarthikeyan *et al.* 2021). Despite being relatively underexplored, YbSnO demonstrates strong potential in biomedical applications. These nanoparticles are capable of absorbing near-infrared (NIR) light, a non-ionizing method that enables deep tissue imaging and photothermal therapy. Upon NIR exposure, YbSnO nanoparticles generate localized heat that can selectively destroy cancer cells while preserving healthy tissue (Eells *et al.* 2004). Previous studies demonstrated that composites like Hydroxyapatite/Yb2O3/Graphene oxide achieved high osteoblast viability, antibacterial efficacy and mechanical performance (Albalwi *et al.* 2022). Similarly, Yb-doped ZnO nanostructures using PVA-assisted methods were synthesized (Lopez *et al.* 2021).

In this work, YbSnO nanoparticles is ongoing, focusing on anticancer efficacy and minimizing their side effects. Furthermore, the biocompatibility and stability of YbSnO nanoparticles are important in biomedical imaging. This study aims to explore the unique properties of nanomaterials for improved biomedical applications, paving the way for future advancements in personalized medicine and therapeutics. Then the A549 cells planted at a density of 5 x 10^6 cells per well in 100 mm culture plates had their gene expression investigated using RT-PCR. Total RNA was isolated from overnight incubated cells using the Total RNA Isolation Reagent (TRIR; Abgene, UK).

2. EXPERIMENTAL SECTION

2.1 Materials

Ytterbium(III) chloride ($YbCl_3$), sodium stannite trihydrate ($Na2SnO_3{\cdot}3H_2O$), urea (CH4N2O), ethanol (C_2H_6O) and nanofiber cellulose (microcrystalline structure; average size 51 µm) were obtained from Sigma-Aldrich. Total RNA Isolation Reagent (TRIR) was obtained from Abgene, UK. All chemicals were used in the experiments without further purification.

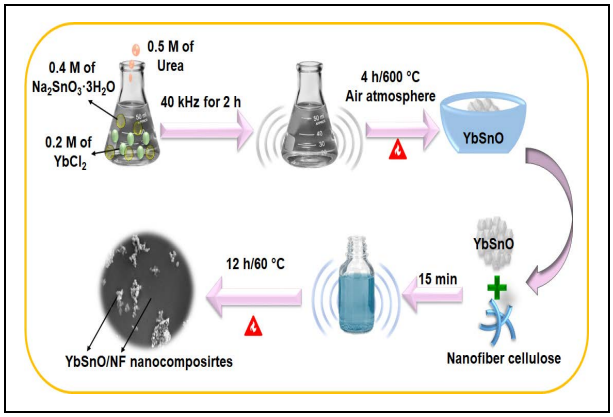


Fig. 1: Synthesis of YbSnO decorated with nanofiber cellulose composites

2.2 Synthesis of YbSnO Nanoparticles

A 0.2 M solution of YbCl3 (2.712 g) was prepared in 35 mL of distilled water and subjected to ultrasonication. Subsequently, a 0.4 M solution of Na2SnO3·3H2O (3.734 g) in 35 mL of distilled water was slowly added dropwise to the YbCl2 solution. Simultaneously, 0.5 g of urea dissolved in 10 mL of

distilled water was added dropwise under continuous ultrasonication for 120 min at room temperature. The resultant homogeneous mixture was washed several times with deionized (DI) water and ethanol, followed by centrifugation at 5000 rpm for 20 min. The mixture was then dried at 80°C for 24 hours. The dried powder was further treated at 600 °C for 5 hours in an air atmosphere ($Yb_2(Sn_2O_7)$ referred to as YbSnO (Fig. 1).

2.3 Preparation of YbSnO/NFC Composites

Typically, 500 mg of YbSnO was dispersed in 30 mL of DI water (solution A) under ultrasonication. Similarly, 50 mg of nanofiber cellulose was dispersed in 10 mL of DI water (solution B). Solution B was stirred while solution A was added dropwise over 2 hours. The resultant mixture was washed five times with DI water to remove unreacted nanofiber cellulose and then air-dried in an oven for 24 hours (Scheme 1). The YbSnO/NFC composites obtained were used for various spectroscopic analyses and biological activity studies.

2.4 Characterization of Prepared Samples

The morphology of prepared samples was examined by field emission scanning microscopy (FE-SEM, Carl Zeiss- Sigma 300; Resolution: 1.0 nm @ 15 kV, 1.6 nm @1kV acceleration voltage: 0.02 kV to 30 kV). The XRD analysis was performed using a Bruker D8 diffractometer over a 2θ range 10° to 80°, with a scan rate of 0.04 seconds. X-ray photoelectron spectroscopy (XPS) was conducted using a Thermo Scientific Multilab 2000 system.

2.5 MTT Assay

To evaluate the cytotoxic effects of rutin on the HT-29 cell line, an MTT assay was conducted. The experimental procedure began with seeding an initial population of 1 × 104 cells, which were allowed to incubate overnight. After this incubation, the MTT reagent was added to the cell culture, and the resulting formazan crystals were solubilized using dimethyl sulfoxide. The absorbance was then measured at 590 nm. The cell viability percentage (Y-axis) was plotted against different concentrations of the samples (X-axis). Concentration of the samples used in the experiment ranged from 0 to 150 µg/mL.

2.6 Gene Expression by RT-PCR

A549 cells were seeded at a density of 5 × 106 cells per well in a 100 mm plate. After an overnight incubation, RNA was extracted using TRIR. The concentration of the extracted RNA was quantified spectrometrically in micrograms (µg). Subsequently, 2 µg of total RNA was reverse transcribed to synthesize complementary DNA (cDNA) following the method described by (Jayaraman *et al.* 2024). In Table 1 for mRNA expression analysis via Real-Time PCR, a reaction mixture was carefully prepared using Takara SyBr Green master mix, along with custom-designed forward and reverse primers. The thermal cycling protocol included an initial activation step of 5 minutes at 95°C, followed by 30 cycles of a two-step process: denaturation for 5 seconds at 95°C and combined annealing and extension for 8 seconds at the designated primer temperature, which ranged from 56 to 65°C.

3. RESULTS AND DISCUSSION

3.1 XRD and FTIR Analysis

Fig. 2 presents the XRD patterns of YbSnO, NFC, and the YbSnO@NFC composite. This analysis provides insights into the structural and bonding characteristics of the synthesized materials. In the XRD pattern of the YbSnO@NFC composite (shown in green, Figure 2a), distinct diffraction peaks from both NFC and YbSnO are clearly observed. The peaks associated with NFC match reference pattern No. 50-2241 from the JCPDS-ICDD, confirming its crystalline nature. In addition to the NFC peaks, well-defined diffraction peaks corresponding to YbSnO are also present. These align well with PDF card No. 01-087-1226, indicating that YbSnO has been successfully incorporated onto the NFC without altering its crystalline phase. This structural integrity demonstrates the compatibility between YbSnO and NFC, as the YbSnO component retains its pyrochlore structure even when integrated into the composite.

The green FTIR spectrum of the YbSnO@NFC composite (Figure 2b) exhibits distinct absorption bands characteristic of YbSnO, along with features potentially attributed to the NFC substrate. In the pure YbSnO spectrum (blue), strong absorption bands appear around 600 cm^{-1} and 450 cm^{-1}, corresponding to the stretching vibrations of Sn–O and Yb–O bonds, respectively. These bands confirm the presence of the YbSnO pyrochlore structure, consistent with the XRD results. In contrast, the red spectrum representing NFC shows minimal absorption below 1000 cm^{-1}, as NFC lacks prominent FTIR-active modes in this region. The dominant features observed in the YbSnO@NFC composite are therefore primarily due to the YbSnO component, indicating successful incorporation without significant interference from the NFC substrate. Overall, the FTIR spectra confirm the presence of metal–oxygen bonds (Sn–O and Yb–O), while the XRD patterns validate the retention of the YbSnO crystalline phases. Together, these findings demonstrate that the YbSnO@NFC composite preserves the structural and compositional integrity of YbSnO, highlighting its suitability for applications requiring stable crystalline materials.

Table 1. RT-PCR primers

S. No.	Name (5' - 3')	Sequence	References
1.	BAX-F BAX-R	TTCTGACGGCAACTTCAACTG TGAGGAGTCTCACCCAACCA	Chen *et al.* (2015)
2.	BCL2-F BCL2-R	GACGCTTTGCCACGGTGGTG GGGGCAGGCATGTTGACTTCAC	Chen *et al.* (2015)
3.	CASP3-F CASP3-R	CTTCAGTGGTGGACATGACG TCAACAATTTGAGGCTGCTG	Yan *et al.* (2009)
4.	mTOR-F mTOR-R	GCTTGATTTGGTTCCCAGGACAGT GTGCTGAGTTTGCTGTACCCATGT	Riquelme *et al.* (2016)
5.	CDKN1A-F CDKN1A-R	TGTCCGTCAGAACCCATGC AAAGTCGAAGTTCCATCGCTC	Sun *et al.* (2018)
6.	β-actin -F β-actin -R	AACAAGATGAGATTGGCA AGTGGGGTGGCTTTTAGGAT	Chen *et al.* (2015)

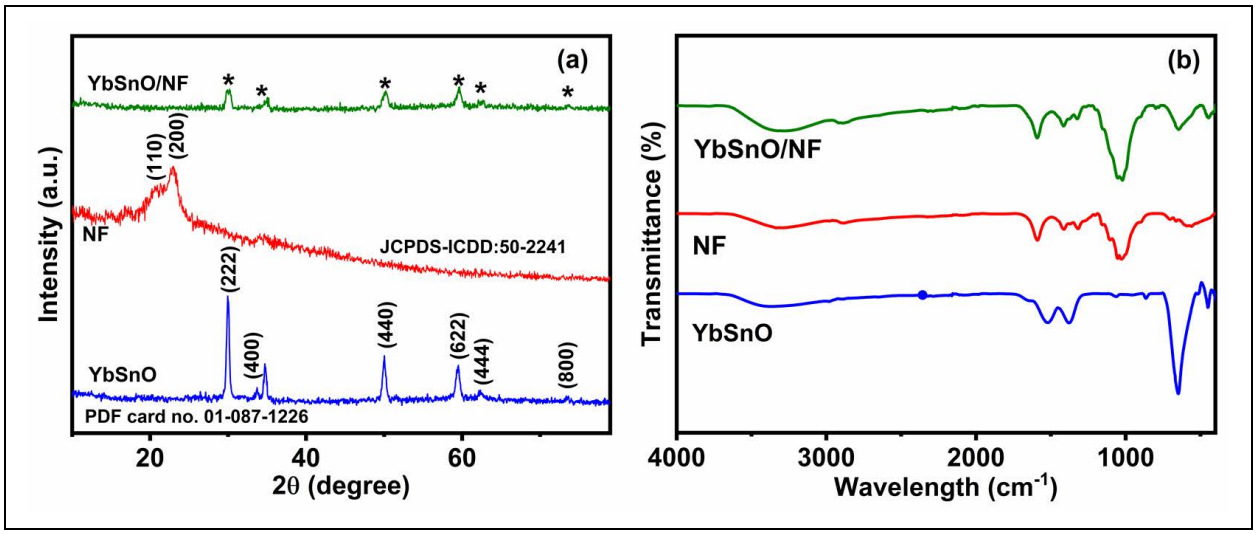


Fig. 2: (a) XRD pattern and (b) FTIR spectrum of YbSnO, NFC, and YbSnO/NFC composites

3.2 Morphological Analysis

A comprehensive morphological and compositional analysis of YbSnO, NFC, and YbSnO@NFC composite was conducted using FE-SEM and EDX, as shown in the accompanying images. The FE-SEM micrograph of pure YbSnO (Figure 3a) reveals a surface composed of agglomerated nanoparticles with a rough, porous texture. This granular morphology suggests a high surface area, which can provide numerous active sites for reactions—an advantageous feature for applications such as biological activity. In Figure 3b, NFC displays a smooth, interconnected fibrous network characteristic of cellulose. This structure offers excellent surface interaction and good biological stability, making it a suitable substrate for supporting composite materials like YbSnO. Figure 3c illustrates the YbSnO@NFC composite, where YbSnO nanoparticles are uniformly distributed across the fibrous NF surface. The nanoparticles adhere well to the Ni foam, maintaining their granular morphology while integrating seamlessly into the fibrous matrix. This uniform dispersion suggests that the composite benefits from both the high surface area of YbSnO and the electrical conductivity of NFC, potentially leading to enhanced electrochemical performance. Figure 3d further confirms the successful synthesis of the YbSnO@NFC composite by showing the homogeneous elemental distribution of ytterbium (Yb), tin (Sn), carbon (C), and oxygen (O). The absence of noticeable phase segregation or particle clustering indicates a well-integrated composite structure, which is essential for achieving consistent electrochemical activity throughout the material. The EDX spectrum of pure YbSnO (Figure 3e) exhibits strong peaks for Yb, Sn, and O, verifying the successful formation of the YbSnO phase with high purity, as no other significant elemental signals are detected. In contrast, the EDX spectrum of NFC (Figure 3f) shows a dominant carbon peak, consistent with the carbon-rich nature of the nanofiber substrate and confirming its

composition. Finally, the EDX spectrum of the YbSnO@NFC composite (Figure 3g) displays characteristic peaks for Yb, Sn, O, and C, confirming the successful integration of YbSnO onto the NFC substrate. The concurrent presence of both YbSnO and NFC components verifies the effective deposition of a substantial amount of YbSnO onto the well-distributed composite material.

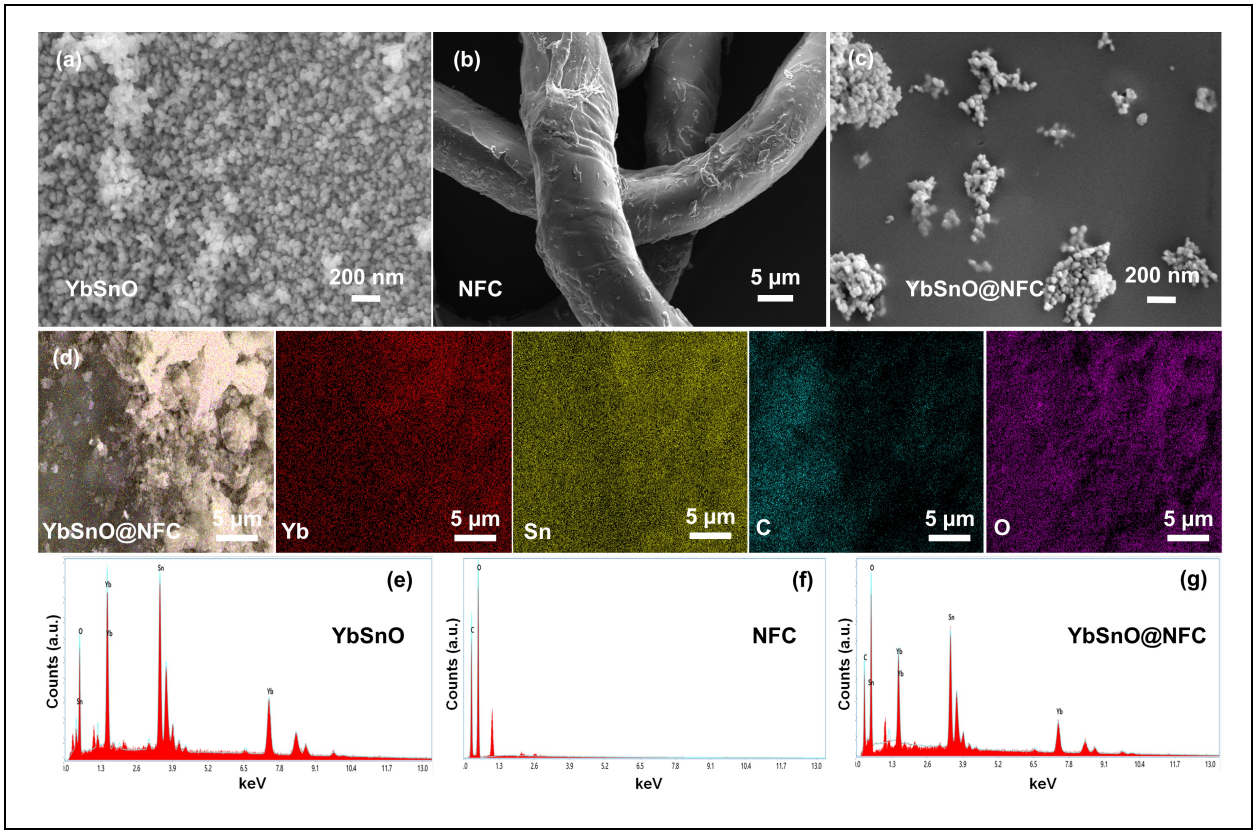


Fig. 3: FE-SEM images of (a) YbSnO (b) nanofiber cellulose (c) YbSnO/NFC composites (d) EDX mapping of YbSnO/NFC composites to present elements for Yb, Sn, C and O. EDX spectrum of (e) YbSnO (f) NFC and (g) YbSnO/NFC composites

3.3 XPS Analysis

The XPS study of YbSnO@NFC composite is shows in the provided Figure 4. This analysis sheds light on the chemical states of the constituent elements, which include ytterbium (Yb), tin (Sn), carbon (C), and oxygen (O). To help identify the bonding environments and oxidation states of the various elements within the composite, each panel Figure 4(a-d) depicts the deconvoluted XPS peaks corresponding to those elements. The binding energies for the Yb 4d area are displayed in Figure.4a of the XPS spectrum. Yb 4d3/2 and Yb 4d5/2, two prominent peaks, are detected at roughly 185 eV and 192 eV, respectively. These energy levels align with the typical energy levels of Yb when it is in its +3 oxidation state. The various sub-peaks shown by the peak fitting may be attributable to Yb's interaction with oxygen and other elements in the YbSnO/NF composite matrix. The sub-peaks observed in the spectra indicate the presence of distinct bonding environments for Yb, confirming that Yb exists in a stable oxidized state within the composite. In the Sn 3d spectra shown in Figure 4b, two prominent peaks appear at binding energies of approximately 487 eV and 495 eV, corresponding to Sn $3d_{5/2}$ and Sn $3d_{3/2}$, respectively. These peaks are characteristic of tin in the +4 oxidation state (Sn^{4+}), specifically in the form of SnO_2. The energy separation (δ) of 8.42 eV between the Sn $3d_{5/2}$ and $3d_{3/2}$ peaks further confirms that Sn is present as Sn(IV) in the composite. This indicates that tin in the YbSnO/NFC composite exists predominantly as SnO_2, which likely contributes to its electrical and structural properties. Figure 4c presents the C 1s spectrum, which exhibits several peaks corresponding to different carbon bonding states. The primary peak at approximately 284.7 eV is attributed to C–C bonds, including both sp^2 and sp^3 hybridized carbons—typical of carbon-based materials such as NFC. Additional peaks at 286.35 eV and 289.02 eV correspond to C–O–C and –COOH groups, respectively. These features indicate the presence of oxygen-containing functional groups on the carbon surface, likely arising from the NFC component or surface modification. Such functional groups can enhance the composite's hydrophilicity and facilitate

charge transfer, potentially influencing its biological activity. In Figure 4d, the O 1s spectrum reveals three distinct peaks, each representing different oxygen species within the composite. The peak at 529.93 eV (O I) is assigned to lattice oxygen (O^{2-}), indicating strong metal–oxygen bonding, likely originating from metal oxides such as SnO_2 and Yb_2O_3. The second peak at 531.39 eV (O II) is attributed to surface hydroxyl groups (–OH), which may result from hydroxylated carbon in NFC or adsorbed water. The third peak, observed at 532.49 eV (O III), corresponds to oxygen in molecularly adsorbed water or oxygen-containing organic species. This further supports the contribution of NFC and surface functionalization to the chemical environment within the composite.

3.4 MTT Assay

In Figure 5 provided is a part of an MTT assay analysis that evaluates the cytotoxic effects of three different samples on the HT-29 cell line. The key components that need to be scientifically explained in Figure 5: (i) The y-axis represents the cell viability percentage. This indicates the proportion of living cells in relation to the total cell population at different concentrations of the samples. A higher percentage means more viable cells, while a lower percentage indicates increased cytotoxicity and cell death. (ii) The x-axis shows the concentration of the samples used in the experiment. It ranges from 0 to 150 µg/mL. Higher concentrations can lead to more cytotoxic effects on the cells, decreasing their viability, as reflected in the declining trend in the graph.

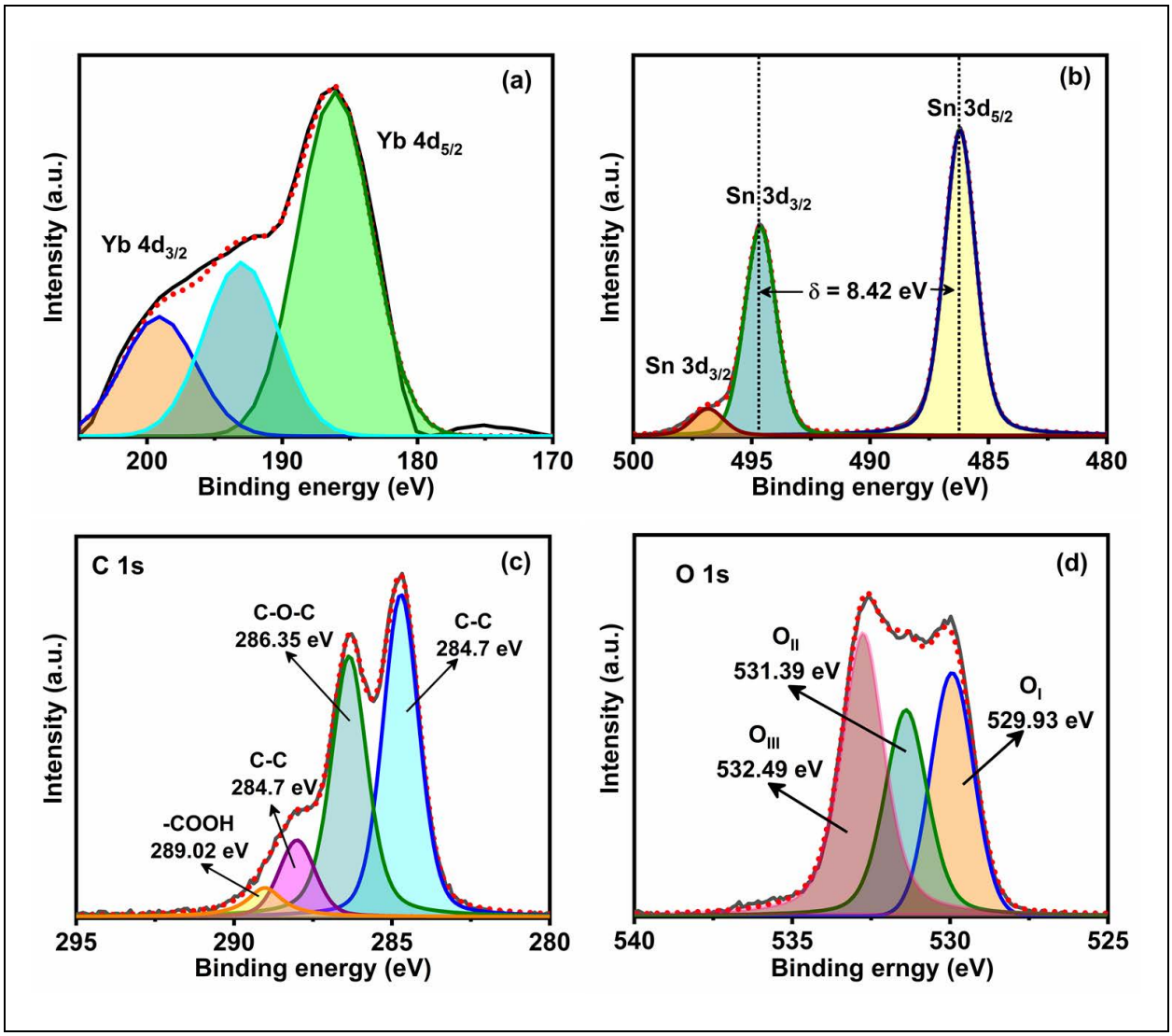


Fig. 4: XPS fitting spectrum of YbSnO/NFC composites from (a) Yb 4d, (b) Sn 3d (c) C 1s and (d) O 1

.

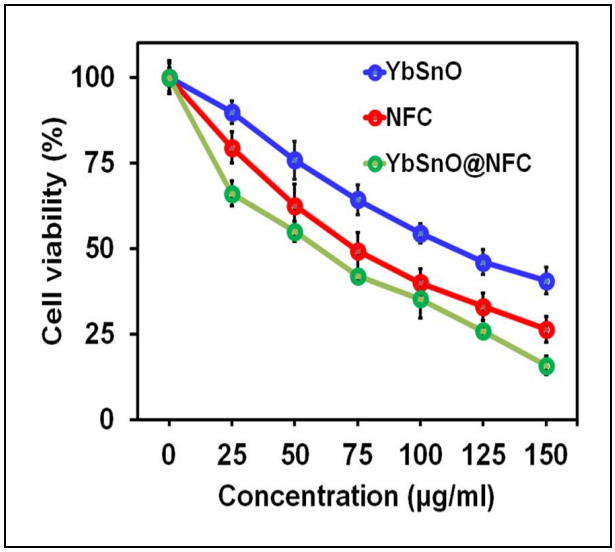


Fig. 5: Cytotoxic effect of nanofibrous composites (sample 1), YbSnO (sample 2) and YbSnO@NFC (sample 3) on the HT-29 cell line.

Fig. 5 illustrates a dose-dependent decrease in cell viability for all three samples, indicating that higher concentrations lead to increased cytotoxicity. Among the samples, NFC shows the least cytotoxicity and the most gradual reduction in cell viability, suggesting its relative biocompatibility. YbSnO exhibits moderate cytotoxicity—greater than NFC but lower than the YbSnO@NFC composite. Notably, the YbSnO@NFC composite demonstrates the highest cytotoxicity, causing the most significant reduction in cell viability. This may suggest a synergistic or enhanced interaction between YbSnO and NFC, leading to increased cytotoxic effects. These findings are critical for assessing the potential biomedical applications of these materials. For instance, as shown in Fig. 6(a–c), samples with lower cytotoxicity may be suitable for drug delivery systems or tissue engineering scaffolds, where biocompatibility is essential. In contrast, more cytotoxic materials like YbSnO@NFC could be advantageous for applications such as cancer therapy, where selective cytotoxicity toward cancer cells is desirable. Additionally, the study evaluates the cytotoxic effects of rutin, a bioactive compound, in combination with these samples. Understanding the cytotoxic profile of each material is crucial for determining their therapeutic index and ensuring safety in biomedical applications.

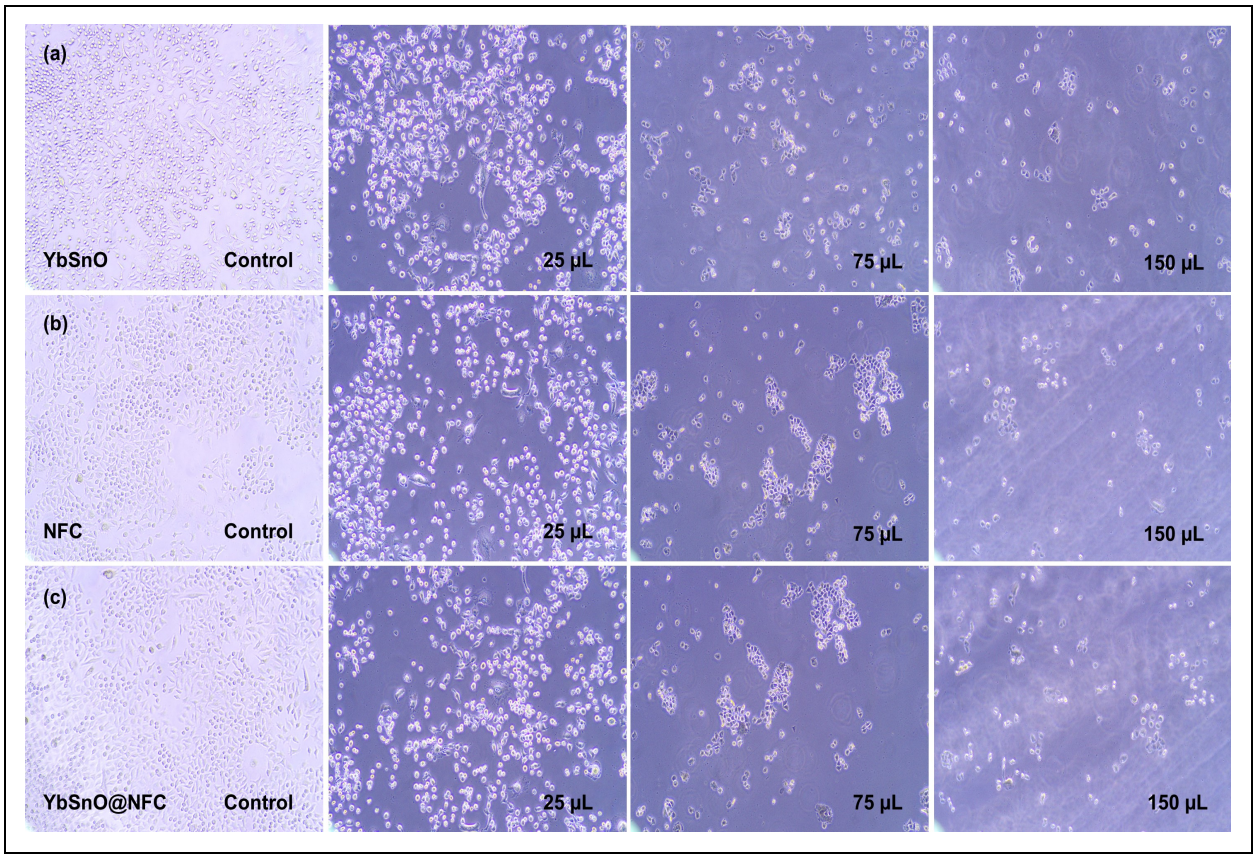


Fig. 6: Cell viability images of HT-29 cells treated with (a) YbSnO, (b) NFC, and (c) YbSnO@NFC composites, compared to the untreated control group

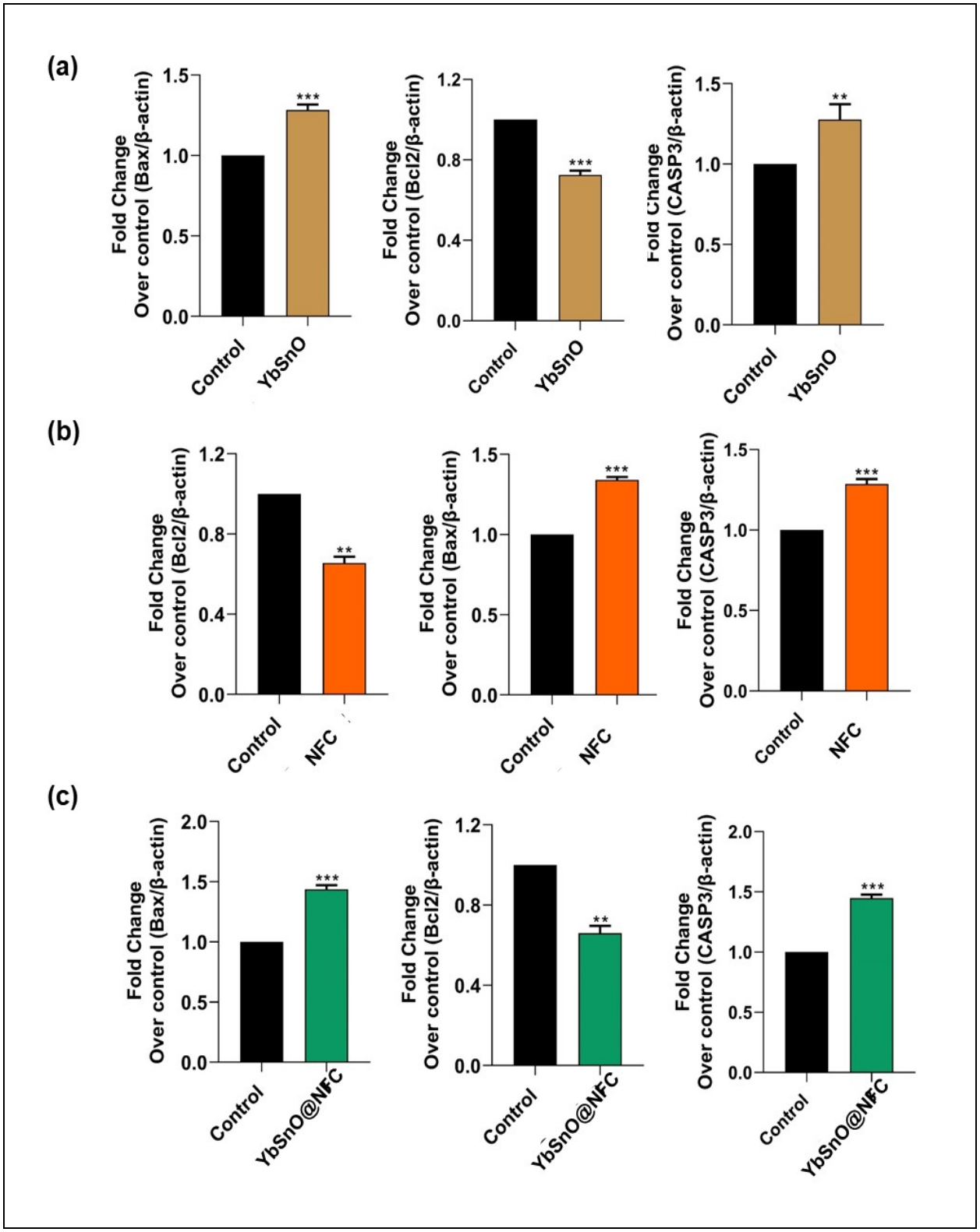


Fig. 7: RT-PCR analysis of gene expression in A549 cells treated with (a) YbSnO, (b) NFC, and (c) YbSnO@NFC. A549 cells were seeded at a density of 5×10^6 cells per well in 100 mm culture plates prior to treatment

In Fig. 7, Quantitative RT-PCR was conducted to investigate the transcriptional responses in A549 cell lines treated with YbSnO, NFC, and YbSnO@NFC composite samples. Following total RNA extraction and cDNA synthesis, validated primers were used to quantify the relative mRNA expression levels of selected genes using the ΔΔCt method. Gene expression was normalized to β-actin, and the results were reported as Bax/β-actin,

Bcl2/β-actin, and CASP3/β-actin ratios. As shown in Figure 7(a-c), gene expression levels varied depending on the treatment. Notably, the expression levels of Bax, Bcl2, and CASP3 were significantly higher—up to several-fold greater—than those observed in untreated controls. This suggests that exposure to YbSnO, NFC, and YbSnO@NFC composites may activate biological pathways related to stress response or apoptosis. These results align with findings from [related condition], where upregulation of similar genes was associated with oxidative stress, apoptosis, and cellular proliferation. However, in some conditions, the expression levels of Bax, Bcl2, and CASP3 were significantly downregulated, suggesting that these genes may also be suppressed through transcriptional inhibition or disruption of associated signaling pathways during sample interaction. Further, mRNA quantification using microarrays revealed a linear correlation between the microarray signal and mRNA concentration. To ensure accurate quantification, the PCR primers were designed to keep gene expression within the linear range of amplification. This may explain why genes with low expression were undetectable by RT-PCR. In cases of moderate gene expression, microarrays might provide a broader dynamic range than PCR. For several genes, poor agreement was observed between RT-PCR and microarray data. Two possible explanations were proposed. First, an increase in "absence" calls (≥1.4 out of 30 data points) for 16 moderately expressed genes—with PCR primers overlapping the microarray probes—significantly reduced the correlation coefficient ($P < 0.05$). Our findings are consistent with other studies reporting that downregulation of Bax, Bcl2, and CASP3 is linked to disease progression and that decreased levels of Gene C can disrupt normal cell cycle regulation and inflammatory responses. Based on these results, [treatment/condition] may alter the regulatory pathways affected by YbSnO, NFC, and YbSnO@NFC composites in A549 cells, potentially impacting their biological functions.

4. CONCLUSION

Summary, we have successfully synthesis of YbSnO@NFCs composites from YbSnO nanoparticles and nanofiber cellulose using simple ultrasonication methods. Asprepared samples were examined the different spectroscopy techniques to confirmed by the morphology, structure and function group present of peak in XPS spectrum. Furthermore, the findings from this graph provide insights into the relative safety and effectiveness of the samples in reducing the viability of HT-29 cells. These results will be crucial in the research article to describe the cytotoxic properties and gene expression using RT-PCR of YbSnO, NFC, and YbSnO@NFCs composites and their potential use in biomedical applications such as cancer therapy or as biomaterials for medical devices.

FUNDING

This research received no specific grant from any funding agency in the public, commercial, or not-for-profit sectors.

CONFLICTS OF INTEREST

The authors declare that there is no conflict of interest.

COPYRIGHT

This article is an open-access article distributed under the terms and conditions of the Creative Commons Attribution (CC BY) license (http://creativecommons.org/licenses/by/4.0/).

REFERENCES

Albalwi, H. A., Naggar, M. E. E., Taleb, M. A., Kalam, A., Alghamdi, N. A., Mostafa, M. S., Salem, S. and Afifi, M., Medical applications of ternary nanocomposites based on hydroxyapatite/ytterbium oxide/graphene oxide: potential bone tissue engineering and antibacterial properties, *J. Mater. Res. Technol.,* 18, 4834–4845(2022). https://doi.org/10.1016/j.jmrt.2022.04.106

Almalki, S. G., The pathophysiology of the cell cycle in cancer and treatment strategies using various cell cycle checkpoint inhibitors, *Pathol. Res. Pract.,* 251, 154854(2023). https://doi.org/10.1016/j.prp.2023.154854

Beheshti, F., Shabani, A. A., Eidgahi, M. R., Kookhaei, P., Vazirian, M. and Safavi, M., Anticancer Activity of Ipomoea purpurea Leaves Extracts in Monolayer and Three-Dimensional Cell Culture, *Evidence-based Complementary Altern. Med.,* 2021, 6666567(2021). https://doi.org/10.1155/2021/6666567

Bhatti, M. M., Sait, S. M. and Ellahi, R., Magnetic Nanoparticles for Drug Delivery through Tapered Stenosed Artery with Blood Based Non-Newtonian Fluid, *Pharm.,* 15(11), 1352(2022). https://doi.org/10.3390/ph15111352

Borges, O., Silva, A. C. D., Tavares, J., Santarem, N., Sousa, A. D., Borchard, G. and Junginger, H. E., Immune response by nasal delivery of hepatitis B surface antigen and codelivery of a CpG ODN in alginate coated chitosan nanoparticles, *Eur. J. Pharm. Biopharm.,* 69(2), 405–416(2008). https://doi.org/10.1016/j.ejpb.2008.01.019

Chen, S., Shuang Z., Xinxing, W., Luo, Z., Enze, J., Yuan, G., Anna, J. S., Hong, Z., Tangfeng, L. and Zhenghong, Yu., Crocin inhibits cell proliferation and enhances cisplatin and pemetrexed chemosensitivity in lung cancer cells, *Translational Lung Cancer Research,* 4(6), 775-83(2015). https://doi.org/10.3978/j.issn.2218-6751.2015.11.03

Cheng, F., Li, W. C., Zhang, W. P. and Lu, A. H., Designed synthesis of nitrogen-rich carbon wrapped Sn nanoparticles hybrid anode via in-situ growth of crystalline ZIF-8 on a binary metal oxide, *Nano Energy.,* 19, 486–494(2016). https://doi.org/10.1016/j.nanoen.2015.10.033

Dheyab, M. A., Aziz, A. A., Jameel, M. S. and Nazila, O., Recent advances in synthesis, modification, and potential application of tin oxide nanoparticles, *Surf. Interfaces.,* 28, 101677(2021). https://doi.org/10.1016/j.surfin.2021.101677

Dsouza, S. and Addepalli, V., Preventive measures in oral cancer: An overview, *Biomed. Pharmacother.,* 107, 72–80(2018). https://doi.org/10.1016/j.biopha.2018.07.114

Eells, J. T., Riley, M. T. T. W., Verhoeve, J., Henry, M., Buchman, E. V., Kane, M. P., Gould, L. J., Das, R., Jet, M., Hodgson, B. D., Margolis, D. and Whelan, H. T., Mitochondrial signal transduction in accelerated wound and retinal healing by near-infrared light therapy, *Mitochondrion.,* 4(5-6), 559–567(2004). https://doi.org/10.1016/j.mito.2004.07.033

Huang, Q., Ding, H. and Razmjooy, N., Oral cancer detection using convolutional neural network optimized by combined seagull optimization algorithm, *Biomed. Signal Process. Control.,* 87, 105546(2024). https://doi.org/10.1016/j.bspc.2023.105546

Jayaraman, S., Natarajan, S. R., Veeraraghavan, V. P. and Jasmine, S., Unveiling the anti-cancer mechanisms of calotropin: Insights into cell growth inhibition, cell cycle arrest, and metabolic regulation in human oral squamous carcinoma cells (HSC-3), *J. Oral. Biol. Craniofac. Res.*, 13(6), 704-713(2023). https://doi.org/10.1016/j.jobcr.2023.09.002

Kaarthikeyan, G., George, P. and Jayakumar, N., Effectiveness of electrospun Ocimum sanctum nanofibers as an adjunct to scaling and root planning in the management of chronic periodontitis, *J. Int. Oral Health.,* 13(2), 115(2021). https://doi.org/10.4103/jioh.jioh_245_20

Kim, S. Y., Doh, H. J., Jang, M. H., Ha, Y. J., Chung, S. I. and Park, H. J., Oral Immunization with Helicobacter pylori-Loaded Poly(d, l-Lactide-Co-Glycolide) Nanoparticles, *Helicobacter.,* 4(1), 33–39(1999). https://doi.org/10.1046/j.1523-5378.1999.09046.x

Lewis, L., Thompson, B., Stellmaker, R. and Koelmeyer, L., Body composition and chemotherapy toxicities in breast cancer: a systematic review of the literature, *J. cancer survivorship: Res. Pract.,* 19(3), 914-929(2025). https://doi.org/10.1007/s11764-023-01512-z

Li, P., Luo, Z., Liu, P., Gao, N., Zhang, Y., Pan, H., Liu, L., Wang, C., Cai, L. and Ma Y., Bioreducible alginate-poly(ethylenimine) nanogels as an antigen-delivery system robustly enhance vaccine-elicited humoral and cellular immune responses, *J. Controlled Release.,* 168(3), 271–279(2013). https://doi.org/10.1016/j.jconrel.2013.03.025

Lopez, D. E. N., Varela, R. G., Sanchez, O. C., Martinez, A. S., Ante, G. S., Romero, K. C., Montoya, D. A. B., Zuniga, A. E. and Mena, E. R. L., Effective antimicrobial activity of ZnO and Yb-doped ZnO nanoparticles against Staphylococcus aureus and Escherichia coli, *Mater. Sci. Eng: C.,* 123, 112004(2021). https://doi.org/10.1016/j.msec.2021.112004

Mira, E. S., Sapri, A. M. S., Aljehani, R. F. and Jambi, B. S., Early Diagnosis of Oral Cancer Using Image Processing and Artificial Intelligence, *Fusion Pract. Appl.,* 14(1), 293–308(2024). https://doi.org/10.54216/FPA.140122

Montalvão, M. F., Gomes, A. R., Guimaraes, A. T. B., Rodrigues, A. S. L., Matos, L. P., Mendonca, J. S., Luz, T. M., Matos, S. G. S., Rahman, M. S., Ragavendran, C., Nathan, S. S., Guru, A., Rakib, M. R. J., Mubarak, N. M. Rahman, M. M., Rocha, T. L., Islam, A. R. M. T. and Malafaia, G., Toxicity of carbon nanofibers in earthworms (Lumbricus terrestris) naturally infected with Monocystis sp, *Sci. Tot. Environ.,* 906, 167712(2024). https://doi.org/10.1016/j.scitotenv.2023.167712

Neto, L. M. M., Zufelato, N., Junior, A. A. S., Trentini, M. M., Costa, A. C., Bakuzis, A. F., Kipnis, A. and Kipnis, A. P. J., Specific T cell induction using iron oxide based nanoparticles as subunit vaccine adjuvant, *Hum. Vaccines Immunother.,* 14(11), 2786-2801(2018). https://doi.org/10.1080/21645515.2018.1489192

Preet, L., Shweta, D. and Ladusingh, R., Diagnostic and therapeutic issues of oral cancer, *Oral Oncol. Rep*., 9(4), 100265 (2024). https://doi.org/10.1016/j.oor.2024.100265

Rajakumar, G., Mao, L., Bao, T., Wen, W., Wang, S., Gomathi, T., Gnanasundaram, N., Rebezov, M., Shariati, M. A., Chung, I. M., Thiruvengadam, M. and Zhang, X., Yttrium Oxide Nanoparticle Synthesis: An Overview of Methods of Preparation and Biomedical Applications, *Appl. Sci.,* 11(5), 2172(2021). https://doi.org/10.3390/app11052172

Riquelme, I., Tapia, O., Espinoza, J. A., Leal, P., Buchegger, K., Sandoval, A. and Roa, J. C., The gene expression status of the PI3K/AKT/mTOR pathway in gastric cancer tissues and cell lines*, Pathol. Oncol. Res*., 22(4), 797-805(2016). https://doi.org/10.1007/s12253-016-0066-5

Saran, M., Zozani, M. A., Behzadifar, M., Gholami, M., Azari, S., Bragazzi, N. L. and Behzadifar, M., Overuse of computed tomography for mild head injury: A systematic review and meta-analysis, *PloS One.,* 19(1), e0293558(2024). https://doi.org/10.1371/journal.pone.0293558

Shabatina, T. I., Vernaya, O. I., Shimanovskiy, N. L. and Melnikov, M. Y., Metal and Metal Oxides Nanoparticles and Nanosystems in Anticancer and Antiviral Theragnostic Agents, *Pharm.,* 15(4), 1181(2023). https://doi.org/10.3390/pharmaceutics15041181

Shabatina, T., Vernaya, O., Shumilkin, A., Semenov, A. and Melnikov, M., Nanoparticles of Bioactive Metals/Metal Oxides and Their Nanocomposites with Antibacterial Drugs for Biomedical Applications, *Mater.,* 15(10), 3602(2022). https://doi.org/10.3390/ma15103602

Siegel, R. L., Giaquinto, A. N. and Jemal, A., Cancer statistics, 2024, *CA Cancer J. Clin.,* 74(1), 12–49(2024). https://doi.org/10.3322/caac.21820

Silva, A. L., Rosalia, R. A., Sazak, A., Carstens, M. G., Ossendorp, F., Oostendorp, J. and Jiskoot, W., Optimization of encapsulation of a synthetic long peptide in PLGA nanoparticles: Low-burst release is crucial for efficient CD8+ T cell activation, *Eur. J. Pharm. Biopharm.,* 83(3), 338–345(2013). https://doi.org/10.1016/j.ejpb.2012.11.006

Sun, X., Yue, H., Jing, W., Liang, S., Lei, Z., Pei-Wen, X., Ji-Fu, W., and Qiang, D., RBMS2 inhibits the proliferation by stabilizing P21 mRNA in breast cancer, *J. Exp. Clin. Cancer Res*., 37, 1-14(2018). https://doi.org/10.1186/s13046-018-0968-z

Thomas, C., Rawat, A., Weeks, L. and Ahsan, F., Aerosolized PLA and PLGA Nanoparticles Enhance Humoral, Mucosal and Cytokine Responses to Hepatitis B Vaccine, *Mol. Pharmaceutics.,* 8(2), 405-415(2011). https://doi.org/10.1021/mp100255c

Tsakiridou, M., Tsagkalias, I., Papi, R. M. and Achilias, D. S., Synthesis of Novel Nanocomposite Materials with Enhanced Antimicrobial Activity based on Poly(Ethylene Glycol Methacrylate)s with Ag, TiO2 or ZnO Nanoparticles, *Nanomater.,* 14(3), 291(2024). https://doi.org/10.3390/nano14030291

Umapathy, V. R., Natarajan, P. M. and Swamikannu, B., Review of the Role of Nanotechnology in Overcoming the Challenges Faced in Oral Cancer Diagnosis and Treatment, *Mol.,* 28(14), 5395(2023). https://doi.org/10.3390/molecules28145395

Vasudevan, A., Majumder, N., Sharma, I., Kaur, I., Sundarrajan, S., Venugopal, J. R., Vijayaraghavan, P., Singh, N., Ramakrishna, S., Ghosh, S., Tripathi, A. M. and Kaur, S., Liver extracellular matrix-based nanofiber scaffolds for the culture of primary hepatocytes and drug screening, *ACS Biomater. Sci. Eng.,* 9(11), 6357–6368(2023). https://doi.org/10.1021/acsbiomaterials.3c01216

Yan, X., Cuiping, F., Qinglin, C., Wentao, L., Hongwei, W., Lihua, Lv., George, W. Smith., Jundong, Wang., Effects of sodium fluoride treatment in vitro on cell proliferation, apoptosis and caspase-3 and caspase-9 mRNA expression by neonatal rat osteoblasts, *Arch. Toxicol.,* 83, 451-458(2009). https://doi.org/10.1007/s00204-008-0365-z

Zhao, L., Seth, A., Wibowo, N., Zhao, C. X., Mitter, N., Yu, C. and Middelberg, A. P. J., Nanoparticle vaccines, *Vaccine.,* 32(3), 327–337(2014). https://doi.org/10.1016/j.vaccine.2013.11.069